Trait-level Attention Control Emerges from Dynamic Frontoparietal Control Network Interactions

Dolly T. Seeburger[1], Jason S. Tsukahara[2], Nan Xu[3], Vishwadeep Ahluwalia[4], Shella D. Keilholz[5], and Randall W. Engle[1]

[1] School of Psychology, Georgia Institute of Technology

[2] Department of Psychology, University of Miami

[3] Fischell Department of Bioengineering, University of Maryland

[4] Center for Advanced Brain Imaging, Georgia Institute of Technology and Georgia State University

[5] Department of Biomedical Engineering, Emory University and Georgia Institute of Technology

Dolly T. Seeburger

Email: dseeburger3@gatech.edu

Author Contributions: D.T.S., J.S.T., and R.W.E. designed research; D.T.S., J.S.T., N.X., and V.W. performed research and analyzed data; S.D.K. and R.W.E. provided methodology; D.T.S. wrote the manuscript; J.S.T., R.W.E., S.D.K., N.X., and V.W. revised the manuscript.

Classification: Psychological and Cognitive Sciences

Keywords: attention control, executive function, brain networks, locus coeruleus, fMRI.

Abstract

Attention control predicts academic achievement, professional success, and health outcomes. However, the neural basis of stable, trait-level differences in attention control remains unclear. Prior research has emphasized momentary fluctuations in attentional engagement, often overlooking enduring individual differences. Here, we applied the quasi-periodic pattern (QPP) analysis of infraslow fMRI dynamics in a large sample (*N* = 191) to test whether trait attention control is reflected in network-level brain activity as well as the locus coeruleus. Using latent-variable measures of attention control, working memory capacity, and fluid intelligence, we isolated the unique contribution of attention control across rest, 1-back, and 3-back conditions. Under heightened cognitive demand, individuals with higher attention control exhibited more flexible coordination of the frontoparietal control network (FPCN): they showed stronger decoupling from the default mode network (DMN), enhanced coupling with the dorsal attention network (DAN), and greater engagement with the locus coeruleus (LC). Even at rest, high attention individuals demonstrated stronger FPCN-DAN coupling, and little to no correlation between FPCN-DMN, indicating that attentional capacity is reflected in both task-evoked reconfiguration and baseline network architecture. These findings reveal how attention control, as a trait, is instantiated in the brain's dynamic architecture.

Significance Statement

Attention control is fundamental to human cognition, and people differ in this trait to maintain focus. These trait-level differences shape success in school, work, and health, but their neural basis has been elusive. Our study shows that attention control is reflected in the brain's dynamic interaction. Individuals higher in attention control demonstrated more flexible coordination between the frontoparietal control network with other attention networks, as well as the locus coeruleus, a major neuromodulatory hub. Furthermore, these signatures are present even in the absence of cognitive load. These findings demonstrate that attention control is not just momentary fluctuations, but a stable trait embedded in large-scale brain dynamics, providing a new framework for understanding the neural organization of individual differences.

Main Text

Introduction

Why attention control matters

Attention control refers to the domain-general ability to focus on goal-relevant information while resisting distraction and interference from task-irrelevant thoughts and events (1,2). It is an ability that has been described as "Supervisory Attentional System" (3), "cognitive control" (4, 5), "executive function" (6), "executive control" (7), "executive attention" (8, 9), and the "central executive" (10). This ability can manifest at both the trait-level - a relatively stable individual difference - and the state-level, where the ability can be diminished due to external distractions and even internal challenges such as fatigue, sleep deprivation, and emotional stress. As a trait variable, it can predict

achievements in academics (11-14), is correlated with mental and physical health (15) , and has positive effects on social and psychological development (16). In adults, it is linked to job performance (17). Despite its broad relevance, the neural basis of stable, trait-level differences in attention control remains poorly understood.

Gaps in prior work and candidate systems

Existing research provides insight into how the average brain responds to fluctuating attentional demands (i.e., state-level variation), however, much less is known about how these responses vary between individuals (i.e., trait-level differences) as well as the interaction between the two factors. This gap in knowledge limits our understanding of the neural basis of individual differences in attention control and constrains the identification of brain-based biomarkers for attention-related disorders. Evidence converges on the prefrontal cortex (PFC) (18) as a central node for maintaining task goals. Thus, it has been proposed that individual differences in attention control are likely mediated by the PFC, particularly the dorsolateral prefrontal cortex (dlPFC) (19). Yet, control is unlikely to be localized to a single region. The frontoparietal control network (FPCN) is a distributed hub that encompasses the dorsolateral and rostrolateral PFC along with areas of the posterior parietal cortex (PPC) including the inferior (IPL) and superior parietal lobule (SPL). Due to its highly connected (20, 21) architecture, the FPCN is the prime candidate to play a central role in coordinating information processing across the brain as a unitary domain general system regulating top-down attention control. It is supported by its connectivity with other networks (22-25), including the default mode network (DMN) (26, 27) involved in internally oriented thought, the dorsal attention network (DAN) (22) which supports externally oriented attention, and the ventral attention network (VAN) (28, 29) which activates during salience detection.

Importantly, the FPCN also maintains reciprocal anatomical connections with the locus coeruleus (LC)(30), the brain's primary source of norepinephrine. Through this neurotransmitter, the LC influences arousal and as a result, brain network reconfiguration. Together, the interaction of networks and the LC provide a plausible mechanism for individual differences in attention control.

QPP framework and the present study

A promising tool for capturing such dynamics is the quasi-periodic pattern (QPP) (31, 32) analysis, which identifies recurring, infraslow spatiotemporal patterns of brain activity. This measure also preserves temporal information and has been shown to account for substantial variance (33) in fMRI signals.

QPPs reveal robust anticorrelations between the DMN and DAN that have been observed at rest (26, 31) and are also linked to task performance (34-38). Weaker anti-correlation has been reported in ADHD patients (39). Moreover, the QPP signatures are shown to be stable within individuals across days (40), raising the possibility that they may index trait-level differences. Yet no study has directly tested whether infraslow network dynamics track stable attentional differences or how these interactions evolve with increasing cognitive demand.

Here, we address this gap by combining a large sample (N = 191), latent-variable modeling of attention control, working memory, and fluid intelligence constructs, and the

QPP analysis across rest, 1-back, and 3-back tasks. This design allows us to isolate the unique contribution of attention control to brain network dynamics and connect trait-level with state-level interactions. We hypothesized that the synchrony of the FPCN with other large-scale networks (DMN, DAN, and VAN), as well as with the LC, would reflect differences in trait-level attention control, and that these differences would become more pronounced under increased task demands.

Results

Latent-variable modeling of cognitive constructs

We first validated the measurement model for attention control, working memory capacity, and fluid intelligence. A three-factor confirmatory factor analysis showed a good fit, $\chi^2(191) = 98.84$, $p < .05$, CFI = .91, RMSEA = .09 [.07, .12]. All factor loadings were significant ($p < .001$). As expected, the latent factors were highly correlated (r = .78–.82) which is consistent with previous studies, known as the positive manifold (45-47); see **Figure 1**. For that reason, to understand if the QPP is indeed capturing attention control, it is crucial to look at attention control's unique contribution. To do so, we removed the shared variance of fluid intelligence and working memory capacity and entered the residualized attention control score into the multilevel-model and compared that to a model using the unresidualized attention control score. Factor loadings and correlations are reported in the **SI Appendix, Table 1** and **Table 2.**

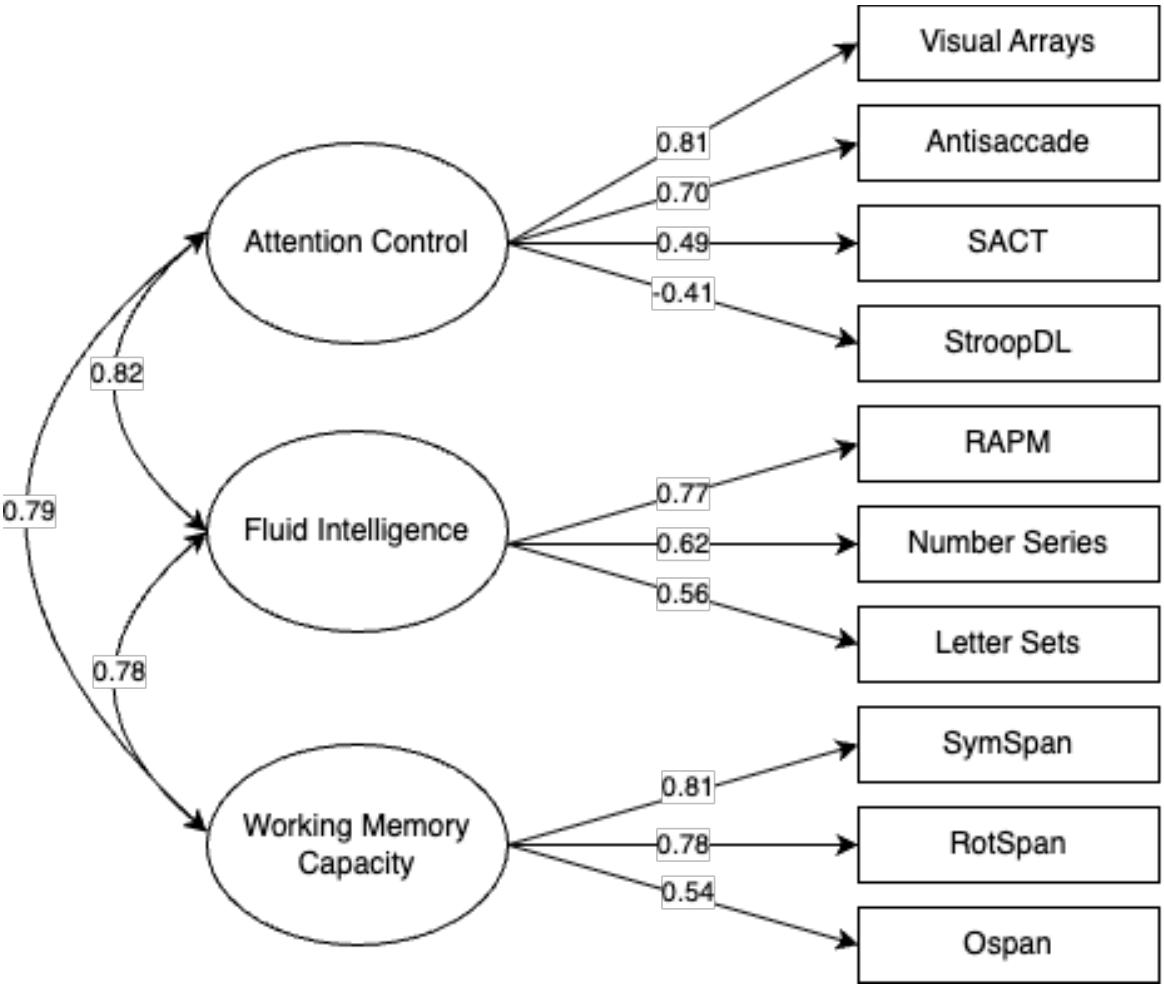

Figure 1. A three factor model using confirmatory factory analysis to capture trait-level attention control, fluid intelligence, and working memory capacity, $\chi^2(191) = 98.84$, $p < .05$, CFI = .91, RMSEA = .09 [.07, .12]. *SACT* Sustained Attention to Cue Task, *StroopDL* Stroop task with an adaptive response deadline, *RAPM* Raven's Advanced Progressive, *SymSpan* Symmetry Span, *OSpan* Operation Span, *RotSpan* Rotation Span.

FPCN–DMN segregation tracks attention control

The FPCN-DMN correlation changed significantly with task demands, $F(2, 191) = 199.13$, $p < .001$, partial $\eta^2 = .014$ and this pattern interacted with attention control uniquely, $F(2, 191) = 30.26$, $p < .001$, partial $\eta^2 = .002$. Participants with higher attention control showed a greater negative FPCN-DMN correlation, particularly in the 3-back condition. Significant interactions were observed across all task pairs (rest vs. 1-back, $p < .001$; 1-back vs. 3-back, $p < .001$; rest vs. 3-back, $p < .001$). For the low attention individuals, during resting state, there was a higher positive FPCN-DMN correlation but as task demands increased, from 1-back to 3-back, that correlation dropped to almost zero. For high attention individuals, during rest, there was an almost zero correlation between FPCN and DMN. As cognitive demand increased in 1-back, it became positively correlated. However, when cognitive load was at its peak, in 3-back, the

correlation turned negative. Lastly, it is worth noting that during the resting state, low attention control participants' FPCN-DMN correlation was more positively correlated than high attention control participants, such that it was statistically different β = –.07, 95% CI [–.09, –.05], *SE* = .01, $t(28{,}586) = -6.74$, $p < .001$; see **Figure 2a.**

Task-dependent FPCN–DAN coupling

The FPCN-DAN correlation changed significantly with task demands, $F(2, 191) = 503.76$, $p < .001$, partial $\eta^2 = .03$ and this pattern interacted with attention control uniquely, $F(2, 191) = 20.87$, $p < .001$, partial $\eta^2 = .001$. Significant differences were found between rest vs. 1-back and 1-back vs. 3-back ($p < .001$). For the low attention individuals, for resting state, the FPCN-DAN was the most anti-correlated but as task demands increased, from 1-back to 3-back, that correlation increased parametrically. For high attention individuals, during rest, there was a slight positive correlation, with minimal changes during 1-back. As cognitive load increased in the 3-back, the FPCN-DAN correlation became very positively correlated. At resting state there was a significant unique effect of attention control on the FPCN-DAN correlation β = .09, 95% CI [.07, .11], $t(28{,}586) = 8.81$, $p < .001$. Low attention control individuals FPCN-DAN were negatively correlated, in contrast with high attention control individuals that were positively correlated; see **Figure 2b.**

FPCN-VAN dynamics and attention control

The FPCN-VAN correlation changed significantly with task demands, $F(2, 191) = 147.84$, $p < .001$, partial $\eta^2 = .01$ and this pattern interacted with attention control uniquely, $F(2, 191) = 37.23$, $p < .001$, partial $\eta^2 = .003$. The FPCN-VAN correlations were significantly different from zero across all task pairs: rest vs. 1-back, rest vs. 3-back ($p < .001$), and 1-back vs. 3-back ($p < .01$). For the low attention individuals, during resting state, the FPCN-VAN were anti-correlated but increased to positively correlating in 1-back, and then back to anti-correlating in 3-back. For high attention individuals, the FPCN-VAN correlation started positive and parametrically decreased to negative from 1-back to 3-back. At resting state there was a significant effect of attention control on the FPCN-VAN correlation β = .07, 95% CI [.05, .09], *SE* = .01, $t(28{,}586) = 6.40$, $p < .001$. Similar to the FPCN-DAN, low attention control individuals' FPCN-VAN were negatively correlated, in contrast with high attention control individuals that were positively correlated; see **Figure 2c.**

Locus coeruleus coupling with the FPCN

The FPCN-LC correlation changed significantly with task demands, $F(2, 191) = 21.58$, $p < .001$, partial $\eta^2 = .002$ and this pattern interacted with attention control uniquely, $F(2, 191) = 38.90$, $p < .001$, partial $\eta^2 = .003$. Significant differences in the FPCN-LC correlations were found for attention control between rest vs. 3-back and 1-back vs. 3-back ($p < .001$). The biggest difference was when task demand was at its highest during 3-back, low attention individuals' FPCN-LC were negatively correlated, while high attention individuals positively correlated. There was no significant effect of attention control on the FPCN-LC correlation during resting state; see **Figure 2d.**

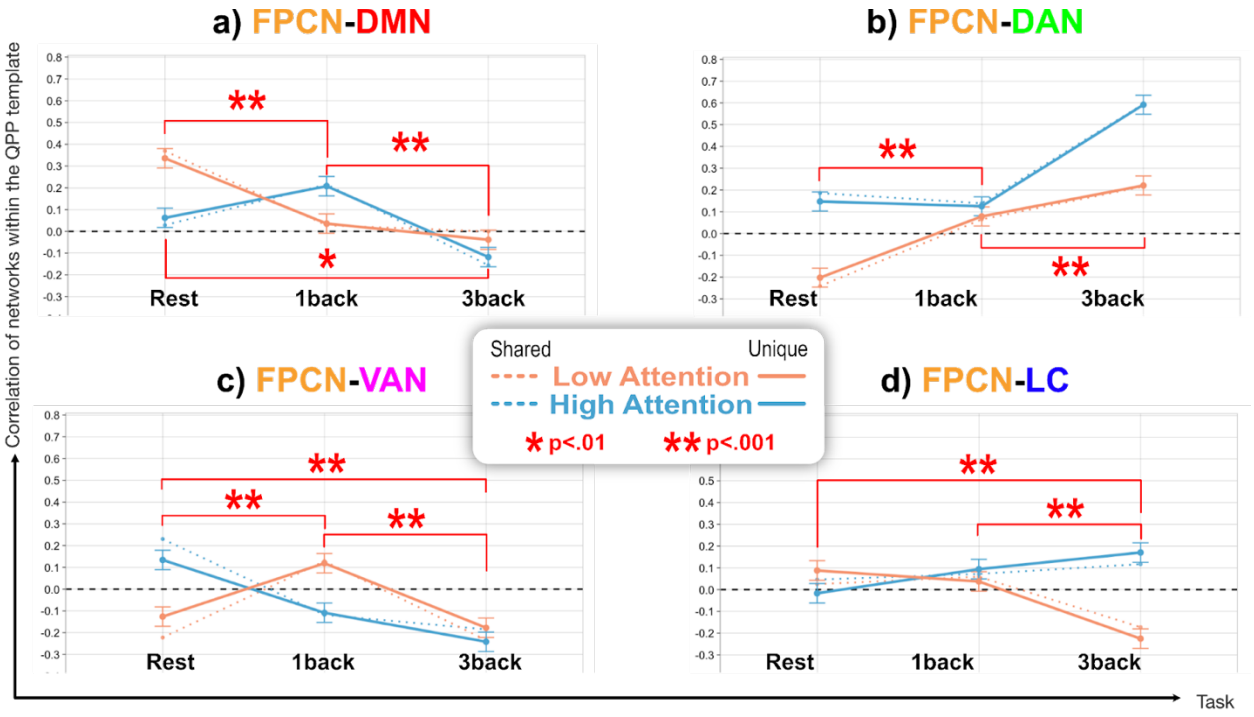

Figure 2. Multilevel modeling results of trait-level attention control, task conditions and the network correlations within the QPP template. **(a)** Correlation of the FPCN-DMN **(b)** Correlation of the FPCN-DAN **(c)** Correlation of the FPCN-VAN **(d)** Correlation of the FPCN- LC within the QPP template. Results visualized as extreme groups with statistics on data from all subjects. High attention are individuals +2SD and low attention are individuals -2SD from the mean. Solid lines indicate unique contribution of attention control (residualized score), dotted lines indicate shared variance of attention control with working memory capacity and fluid intelligence (unresidualized score). *FPCN* frontoparietal control network, *DMN* default mode network, *DAN* dorsal attention network, *VAN* ventral attention network, *LC* locus coeruleus, *QPP* quasi-periodic pattern.

Group-level QPP differences

Group QPP templates confirmed these individual-level effects. During resting state, the low attention control group had a stronger positive FPCN-DMN correlation (Low r = .93) than the high attention control group (High r = .40), but a more negative FPCN-DAN (Low r =–.90 vs. High r =–.30), and FPCN-VAN (Low r =–.79 vs. High r =–.36) correlation. While the FPCN-LC correlation was similar (Low r =.06 vs. High r =.06) correlation. During 1-back, group differences were smaller. Largest differences were observed during the 3-back, where the low attention control group had a weaker FPCN-DMN anti-correlation (Low r =–.60 vs. High r =–.89), a weaker FPCN-DAN positive correlation (Low r =.91 vs High r =.98), and weaker FPCN-VAN negative correlation (Low r =–.69 vs. High r =–.71). For FPCN-LC, the low attention control group showed near-zero correlation (Low r = –.03) compared to a positive correlation in the high group (High r = .63); see **Figure 3.**

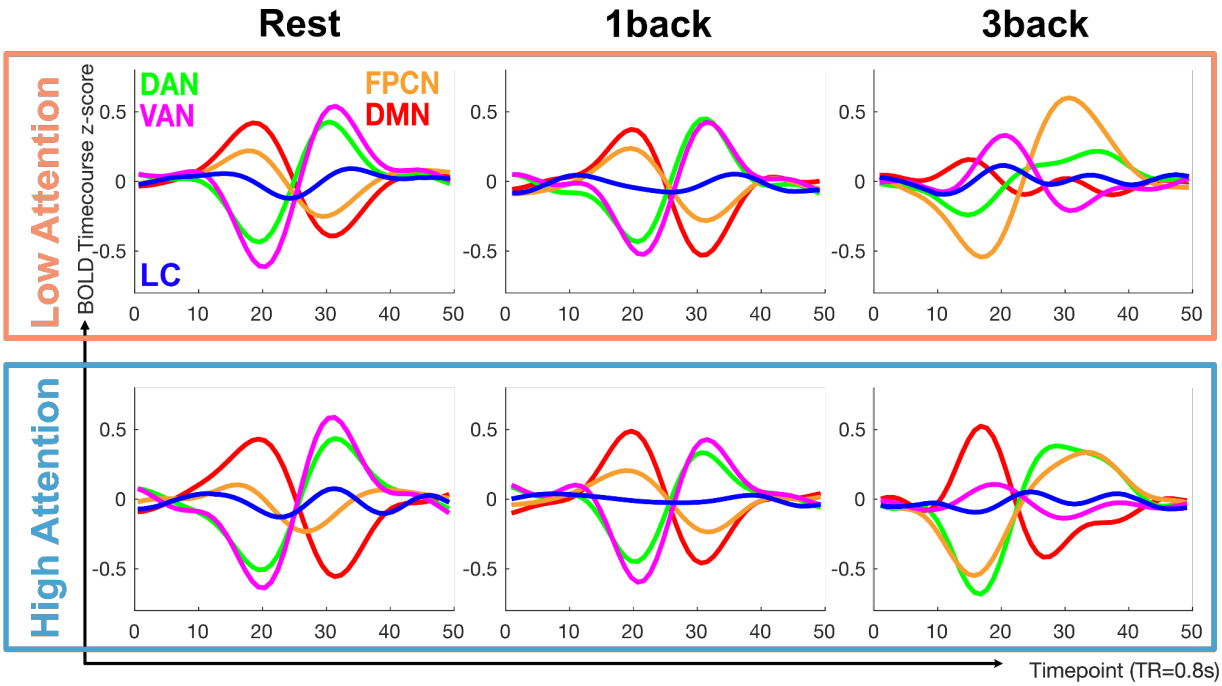

Figure 3. Group level quasi-periodic pattern template results with a tertiary split on the attention control latent factor estimated score (N=63) for high attention and (N=63) for low attention. *FPCN* frontoparietal control network, *DMN* default mode network, *DAN* dorsal attention network, *VAN* ventral attention network, *LC* locus coeruleus.

Discussion

In line with the framework put forward by Spreng and colleagues (23), we demonstrated that the frontoparietal control network (FPCN) functions as a domain-general hub that couples with the default mode network (DMN) or the dorsal attention network (DAN) depending on whether attention is internally or externally oriented (ie., state-level). A key advancement made from this study is the clarification that these dynamics are not merely state-dependent but that they are also shaped by trait-level attention control.

High attention control individuals showed stronger anticorrelation of the FPCN-DMN, especially under increased cognitive load, demonstrating efficient disengagement from internally focused processing when goal-relevant external demands are present. In contrast, low attention control individuals showed less FPCN-DMN segregation, suggesting difficulty disengaging from internal processing when external focus is required.

On the flip side, FPCN-DAN coupling increased with task difficulty across participants, but the trajectory differed by trait attention control. At rest, high attention individuals demonstrated slightly positive FPCN-DAN coupling that sharply increased during the 3-back. Low attention individuals began from a negative baseline and showed a more muted increase, without reaching the synchrony levels of high attention individuals. This pattern suggests that higher attention control is associated with a more "attention-ready" network configuration even at baseline. These results extend prior studies (25, 48, 38) by showing that dynamic flexibility is not only state-dependent but also varies by trait-level and is evident even at rest.

A more complex pattern emerged for interactions between the FPCN and the ventral attention network (VAN). At rest, high attention individuals exhibited positive correlation of the FPCN-VAN, and decreased as cognitive load increased. In contrast, low attention individuals showed a more complicated pattern - negative at rest to positive during 1 back to negative again at 3 back. This pattern aligns with a previous within subject study in which the researchers (38) found that during sustained "in-the-zone" states, the FPCN decouples from the VAN while the VAN increases synchrony with the DMN.

In the 3-back condition, high attention control individuals showed robust positive coupling between the FPCN and locus coeruleus (LC), whereas low attention participants exhibited weak or negative coupling; these effects were not observed at rest. This indicates that FPCN–LC coordination is particularly important under high cognitive load. The result aligns with animal work showing that LC firing (49, 50) increases with task difficulty and tracks behavioral response demands, and with human pupillometry showing that pupil dilation increases with cognitive effort and predicts performance (51) . Pupillometry, which serves as a proxy for LC-norepinephrine activity, has also shown that pupil dilation increases with cognitive effort and can predict task performance (52). Given the LC's extensive noradrenergic projections and bidirectional interactions with prefrontal cortex, these findings suggest that trait-level attention control emerges not only from flexible coordination of large-scale brain networks but also the capacity to dynamically recruit the LC as cognitive load increases. Although traditionally linked to arousal, the LC likely plays a central role in supporting complex cognitive functions, including attention control, via modulation of FPCN dynamics.

Despite high correlations among latent factors of attention control, working memory capacity, and fluid intelligence, we are confident that the QPP, which captures infraslow brain activity via fMRI, reflects something distinctively related to attention control. Our multilevel modeling includes the residualized score of attention control independent of shared variance with working memory capacity and fluid intelligence; in other words, we isolate the contribution of attention control and still find significant interactions. This fits with accounts suggesting that attention control is a foundational mechanism underpinning both working memory capacity and fluid intelligence (1, 2, 9, 53, 54).

Taken together, these findings provide converging evidence that QPP-derived dynamics capture both state and trait-like neural signatures specific to attention control. While interrelated with working memory and fluid intelligence, attention control appears to leave a unique footprint in the brain's intrinsic and task-evoked temporal architecture - one that QPP analysis is well-suited to detect.

Implications

These findings bridge trait and state perspectives and advances our understanding of how cortical and neuromodulatory systems jointly support attention control. In addition, this highlights potential biomarkers of attentional control with direct relevance for mental health and applied performance contexts.

Limitations and future directions

Several limitations should be noted. The locus coeruleus is small and anatomically variable, and our use of a standardized mask in MNI space introduces some imprecision; subject-specific neuromelanin images would provide greater accuracy. Secondly, global signal regression (GSR) remains controversial due to concerns that it may artificially induce anticorrelations or obscure meaningful global fluctuations. However, researchers (55) suggest that the global signal may obscure underlying neurophysiology and its removal can be useful. Future work could examine interindividual differences in the global signal characteristics - potentially offering another marker of trait-level differences. Third, while comparing 1-back and 3-back conditions gives us a window into state-level changes of brain dynamics, it's important to acknowledge that these tasks aren't just harder or easier versions of the same task, as they likely engage different strategies altogether. Future research would benefit from a more adaptive task design, titrated to each participant's performance level, to more precisely capture how attention networks and the LC respond to increasing cognitive demands. Finally, the relationships we observed are correlational and should not be interpreted as causal. Interventional work such as pharmacological modulation or noninvasive brain stimulation targeting the FPCN and LC would be valuable in testing whether changes in connectivity between these neural pathways actively supports attentional control or merely reflects it.

Conclusion

By combining latent-variable modeling, quasi-periodic pattern analysis, and a large fMRI sample, this study identifies a dynamic neural signature of trait-level attention control. Stronger FPCN-DMN segregation, greater FPCN-DAN and FPCN-LC coupling, especially under high load, together provide a mechanistic account of why some individuals are better able to control their attention. Furthermore, these neural signatures were apparent during rest, indicating a possible task-ready state that high attention individuals may possess. This trait and state interaction underscores the dynamic nature of attentional processes in that state-level adaptations appear scaffolded by stable trait-level individual differences in neural organization.

Materials and Methods

Participants

Two hundred eighteen adults participated in a three-session study consisting of two behavioral sessions and one MRI session. Participants were between 18 and 35 years old, with strong right-handedness, no color-blindness, no history of seizures, no neurological issues, and were MRI safe. Recruitment included both Georgia Tech students (52.4%) and community members (47.6%). Compensation was scaled by session. Exclusions due to incomplete data, structural anomalies, excessive motion, or missing behavioral results yielded a final sample of N = 191 (57% female; M = 23.6 years, SD = 4.7).

Cognitive measures

Latent factors of attention control, working memory capacity, and fluid intelligence were each assessed outside the fMRI scanner with multiple tasks on two separate days. Data were cleaned for chance performance and outliers. Confirmatory factor analysis (41) was used to extract the three factors, and scores were estimated for each individual using the Bartlett (42) method. Details of the tasks design and behavioral data processing are reported in the SI Appendix.

fMRI acquisition

MRI data were acquired on a 3T Siemens Magnetom Prisma^{fit} MRI with a 32-channel head coil at GSU/GT Center for Advanced Brain Imaging, Atlanta. 3D T1-weighted MPRAGE and 3D T2-weighted SPACE scans were acquired at 0.8mm^3 resolution. The task-fMRI and rest-fMRI scans were acquired using a multiband GRE-EPI sequence with the following parameters: 750 volumes, 72 slices, TR = 800 ms, TE = 37.40 ms, field of view = 208×208mm, voxel dimensions = 2.0×2.0×2.0 mm, MB = 8. The order of these runs was counterbalanced in the study. Participants were instructed to keep their eyes open and focused on a fixation cross during the 10 minute resting-state (no-load condition). The 1-back (low-load condition) and 3-back (high-load condition) tasks were based on the Human Connectome Project n-back protocol and were acquired separately with a duration of 10 mins each. The participants practiced the n-back tasks prior to entering the MRI. Details of the task design are reported in the **SI Appendix.**

Preprocessing

Data were preprocessed using the Configurable Pipeline for the Analysis of Connectomes (C-PAC) (43). Steps included bias correction, skull stripping, slice-timing and distortion correction, motion correction, MNI registration, nuisance regression (including global signal regression), temporal bandpass filtering (0.01–0.1 Hz), quadratic detrending, and spatial smoothing (4 mm FWHM). Following head motion guidelines (32), 5 participants with mean framewise displacement > 0.12 mm and 40% of frames > 0.2 mm were excluded from the analysis.

Quasi-periodic pattern (QPP) analysis

A pattern-finding algorithm originally described by Majeed and colleagues (2011) and further refined by others (40, 44) was applied separately to each participant's functional scan - resting state, 1-back, and 3-back. Each scan was 10 mins (volumes = 750). The QPP detection algorithm can be summarized in these steps. First, it selects an initial spatiotemporal brain pattern of 20 s (timepoints = 25, TR = 800 ms) of each brain scan. Second, it uses a sliding window correlation to iteratively search across the scan for spatiotemporal patterns where the BOLD signal correlates, at a threshold of local maxima of $r = 0.2$, with the initial pattern. Third, as the correlating patterns are identified, they are averaged into the original pattern (updating the pattern as the search progresses). This process continues until the end of the brain scan. Steps 1-4 were repeated for all starting timepoints excluding the last 20 s within each participant. Lastly, the number of instances where the BOLD signal correlates above threshold for each different spatiotemporal pattern is calculated and ranked. The pattern with the highest sum occurrence is selected as the QPP template for each functional scan for each participant. In this way, the algorithm identifies the most commonly repeating pattern of network activity for each subject and each task. Within this QPP template is where correlation time courses between the FPCN and DMN, DAN, VAN, and LC were extracted for each subject and load condition. Group-level QPPs were generated from tertile splits on the trait-level attention control latent construct by concatenating the scan time series of individuals in the extreme groups. The top third percentile group served as the high attention control group (n=63) while the bottom third percentile served as the low attention control group (n=63). A detailed process flowchart of the QPP analysis can be found in Fig.S2 of Yousefi & Keilholz, 2021. The code for QPP analysis is openly available at https://github.com/imnanxu/QPPLab (44).

Statistical analysis

Multilevel linear models were used to test whether FPCN connectivity within the QPP varied by trait-level attention control and load condition. To do so, the average BOLD signal of all the regions of interest (ROIs) from the FPCN was entered as a Level 1 predictor of another network/region of interest - DAN, DMN, VAN, and LC. The load conditions - rest, 1-back and 3-back- were entered as Level 2. While Level 3 was the unresidualized (shared variance) or the residualized (unique variance) trait-level attention control, z-scored. This setup answers the question of the unique contribution of attention control - independent of working memory capacity and fluid intelligence - to the QPP signal as a function of task demands. A stricter alpha threshold ($p < .01$) was used to correct for the multiple comparisons of tasks.

Acknowledgments

This work was supported by the Office of Naval Research Grants N000142212218 and N000142312768 to Randall W. Engle.

References

A. P. Burgoyne, R. W. Engle, Attention control: A cornerstone of higher-order cognition. *Curr. Dir. Psychol. Sci.* **29**, 624–630 (2020).

R. W. Engle, Working memory and executive attention: A revisit. *Perspect. Psychol. Sci.* **13**, 190–193 (2018).

D. A. Norman, T. Shallice, Attention to action: Willed and automatic control of behavior. In R. J. Davidson, G. E. Schwartz, D. Shapiro (Eds.), *Consciousness and Self-Regulation*, pp. 1–18 Springer (1986).

M. M. Botvinick, T. S. Braver, D. M. Barch, C. S. Carter, J. D. Cohen, Conflict monitoring and cognitive control. *Psychol. Rev.* **108**, 624–652 (2001).

T. Egner, Congruency sequence effects and cognitive control. *Cogn. Affect. Behav. Neurosci.* **7**, 380–390 (2007).

A. Miyake, N. P. Friedman, M. J. Emerson, A. H. Witzki, A. Howerter, T. D. Wager, The unity and diversity of executive functions and their contributions to complex “frontal lobe” tasks: A latent variable analysis. *Cogn. Psychol.* **41**, 49–100 (2000).

M. I. Posner, S. E. Petersen, The attention system of the human brain. *Annu. Rev. Neurosci.* **13**, 25–42 (1990).

R. W. Engle, What is working memory capacity? In H. L. Roediger III, J. S. Nairne, I. Neath, A. M. Surprenant (Eds.), *The Nature of Remembering: Essays in Honor of Robert G. Crowder*, pp. 297–314 (American Psychological Association, 2001).

R. W. Engle, Working memory capacity as executive attention. *Curr. Dir. Psychol. Sci.* **11**, 19–23 (2002).

A. Baddeley, Exploring the central executive. (n.d.).

E. Borella, B. Carretti, S. Pelegrina, The specific role of inhibition in reading comprehension in good and poor comprehenders. *J. Learn. Disabil.* **43**, 541–552 (2010).

T. Rohde, L. Thompson, Predicting academic achievement with cognitive ability. *Intelligence* **35**, 83–92 (2007).

F. Spinath, N. Harlaar, R. Plomin, Predicting school achievement from general cognitive ability, self-perceived ability, and intrinsic value. *Intelligence* **34**, 363–374 (2006).

J. A. Welsh, R. L. Nix, C. Blair, K. L. Bierman, N. E. Nelson, The development of cognitive skills and gains in academic school readiness for children from low-income families. *J. Educ. Psychol.* **102**, 43–53 (2010).

H. Miller, Self-control and health outcomes in a nationally representative sample. *Am. J. Health Behav.* **35**, 2 (2011).

A. Diamond, The evidence base for improving school outcomes by addressing the whole child and by addressing skills and attitudes, not just content. *Early Educ. Dev.* **21**, 780–793 (2010).

T. A. Judge, R. L. Klinger, L. S. Simon, Time is on my side: Time, general mental ability, human capital, and extrinsic career success. *J. Appl. Psychol.* **95**, 92–107 (2010).

E. K. Miller, J. D. Cohen, An integrative theory of prefrontal cortex function. *Annu. Rev. Neurosci.* **24**, 167–202 (2001).

M. J. Kane, R. W. Engle, The role of prefrontal cortex in working-memory capacity, executive attention, and general fluid intelligence: An individual-differences perspective. *Psychon. Bull. Rev.* **9**, 637–671 (2002).

S. M. Szczepanski, M. A. Pinsk, M. M. Douglas, S. Kastner, Y. B. Saalmann, Functional and structural architecture of the human dorsal frontoparietal attention network. *Proc. Natl. Acad. Sci. U.S.A.* **110**, 15806–15811 (2013).

T. Liebe, J. Kaufmann, D. Hämmerer, M. Betts, M. Walter, In vivo tractography of human locus coeruleus—relation to 7T resting state fMRI, psychological measures and single subject validity. *Mol. Psychiatry* **27**, 4984–4993 (2022).

M. Corbetta, G. L. Shulman, Control of goal-directed and stimulus-driven attention in the brain. *Nat. Rev. Neurosci.* **3**, 201–215 (2002).

R. N. Spreng, W. D. Stevens, J. P. Chamberlain, A. W. Gilmore, D. L. Schacter, Default network activity, coupled with the frontoparietal control network, supports goal-directed cognition. *Neuroimage* **53**, 303–317 (2010).

A. Fornito, B. J. Harrison, A. Zalesky, J. S. Simons, Competitive and cooperative dynamics of large-scale brain functional networks supporting recollection. *Proc. Natl. Acad. Sci. U.S.A.* **109**, 12788–12793 (2012).

P. J. Hellyer, M. Shanahan, G. Scott, R. J. Wise, D. J. Sharp, R. Leech, The control of global brain dynamics: Opposing actions of frontoparietal control and default mode networks on attention. *J. Neurosci.* **34**, 451–461 (2014).

M. D. Fox, A. Z. Snyder, J. L. Vincent, M. Corbetta, D. C. Van Essen, M. E. Raichle, The human brain is intrinsically organized into dynamic, anticorrelated functional networks. *Proc. Natl. Acad. Sci. U.S.A.* **102**, 9673–9678 (2005).

M. E. Raichle, The brain's default mode network. *Annu. Rev. Neurosci.* **38**, 433–447 (2015).

W. W. Seeley, V. Menon, A. F. Schatzberg, J. Keller, G. H. Glover, H. Kenna, A. L. Reiss, M. D. Greicius, Dissociable intrinsic connectivity networks for salience processing and executive control. *J. Neurosci.* **27**, 2349–2356 (2007).

V. Menon, L. Q. Uddin, Saliency, switching, attention and control: A network model of insula function. *Brain Struct. Funct.* **214**, 655–667 (2010).

A. F. T. Arnsten, P. S. Goldman-Rakic, Selective prefrontal cortical projections to the region of the locus coeruleus and raphe nuclei in the rhesus monkey. *Brain Res.* **306**, 9–18 (1984).

W. Majeed, M. Magnuson, W. Hasenkamp, H. Schwarb, E. H. Schumacher, L. Barsalou, S. D. Keilholz, Spatiotemporal dynamics of low frequency BOLD fluctuations in rats and humans. *Neuroimage* **54**, 1140–1150 (2011).

B. Yousefi, J. Shin, E. H. Schumacher, S. D. Keilholz, Quasi-periodic patterns of intrinsic brain activity in individuals and their relationship to global signal. *Neuroimage* **167**, 297–308 (2018).

A. Abbas, M. Belloy, A. Kashyap, J. Billings, M. Nezafati, E. H. Schumacher, S. D. Keilholz, Quasi-periodic patterns contribute to functional connectivity in the brain. *Neuroimage* **191**, 193–204 (2019).

A. M. C. Kelly, L. Q. Uddin, B. B. Biswal, F. X. Castellanos, M. P. Milham, Competition between functional brain networks mediates behavioral variability. *Neuroimage* **39**, 527–537 (2008).

G. J. Thompson, M. E. Magnuson, M. D. Merritt, H. Schwarb, W. Pan, A. McKinley, L. D. Tripp, E. H. Schumacher, S. D. Keilholz, Short-time windows of correlation between large-scale functional brain networks predict vigilance intraindividually and interindividually. *Hum. Brain Mapp.* **34**, 3280–3298 (2013).

A. Kucyi, M. J. Hove, M. Esterman, R. M. Hutchison, E. M. Valera, Dynamic brain network correlates of spontaneous fluctuations in attention. *Cereb. Cortex* **27**, 1831–1840 (2017).

R. Esposito, F. Cieri, P. Chiacchiaretta, N. Cera, M. Lauriola, M. Di Giannantonio, A. Tartaro, A. Ferretti, Modifications in resting state functional anticorrelation between default mode network and dorsal attention network: Comparison among young adults, healthy elders and mild cognitive impairment patients. *Brain Imaging Behav.* **12**, 127–141 (2018).

D. T. Seeburger, N. Xu, M. Ma, S. Larson, C. Godwin, S. D. Keilholz, E. H. Schumacher, Time-varying functional connectivity predicts fluctuations in sustained attention in a serial tapping task. *Cogn. Affect. Behav. Neurosci.* **24**, 111–125 (2024).

A. Abbas, Y. Bassil, S. Keilholz, Quasi-periodic patterns of brain activity in individuals with attention-deficit/hyperactivity disorder. *Neuroimage Clin.* **21**, 101653 (2019).

B. Yousefi, S. Keilholz, Propagating patterns of intrinsic activity along macroscale gradients coordinate functional connections across the whole brain. *Neuroimage* **231**, 117827 (2021).

Y. Rosseel, lavaan: An R package for structural equation modeling. *J. Stat. Softw.* **48**, 1–36 (2012).

M. S. Bartlett, The statistical conception of mental factors. *Br. J. Psychol.* **28**, 97–104 (1937).

C. Craddock, S. Sikka, B. Cheung, R. Khanuja, S. S. Ghosh, C. Yan, et al., Towards automated analysis of connectomes: The configurable pipeline for the analysis of connectomes (c-pac). *Front. Neuroinform.* **42**, (2013).

N. Xu, B. Yousefi, N. Anumba, T. J. LaGrow, X. Zhang, S. D. Keilholz, QPPLab: A generally applicable software package for detecting, analyzing, and visualizing large-scale quasiperiodic spatiotemporal patterns (QPPs) of brain activity. *SoftwareX* **29**, 102067 (2025).

C. Spearman, “General intelligence,” objectively determined and measured. *Am. J. Psychol.* **15**, 201–293 (1904).

C. Spearman, *The Abilities of Man* (Macmillan, 1927).

A. P. Burgoyne, C. A. Mashburn, J. S. Tsukahara, R. W. Engle, Attention control and process overlap theory: Searching for cognitive processes underpinning the positive manifold. *Intelligence* **91**, 1–11 (2022).

L. J. Hearne, J. B. Mattingley, L. Cocchi, Functional brain networks related to individual differences in human intelligence at rest. *Sci. Rep.* **6**, 1–8 (2016).

J. Rajkowski, H. Majczynski, E. Clayton, G. Aston-Jones, Activation of monkey locus coeruleus neurons varies with difficulty and performance in a target detection task. *J. Neurophysiol.* **92**, 361–371 (2004).

P. Bornert, S. Bouret, Locus coeruleus neurons encode the subjective difficulty of triggering and executing actions. *PLoS Biol.* **19**, e3001487 (2021).

P. Van der Wel, H. Van Steenbergen, Pupil dilation as an index of effort in cognitive control tasks: A review. *Psychon. Bull. Rev.* **25**, 2005–2015 (2018).

J. S. Tsukahara, R. W. Engle, Fluid intelligence and the locus coeruleus–norepinephrine system. *Proc. Natl. Acad. Sci. U.S.A.* **118**, e2110630118 (2021).

C. Draheim, T. L. Harrison, S. E. Embretson, R. W. Engle, What item response theory can tell us about the complex span tasks. *Psychol. Assess.* **30**, 116–129 (2018).

C. A. Mashburn, J. S. Tsukahara, R. W. Engle, Individual differences in attention control. In *Working Memory: The State of the Science* (Oxford University Press, 2020).

M. D. Fox, D. Zhang, A. Z. Snyder, M. E. Raichle, The global signal and observed anticorrelated resting state brain networks. *J. Neurophysiol.* **101**, 3270–3283 (2009).

Supporting Information for

Trait-level Attention Control Emerges from Dynamic Frontoparietal Control Network Interactions

Dolly T. Seeburger, Jason S. Tsukahara, Nan Xu, Vishwadeep Ahluwalia, Shella D. Keilholz, Randall W. Engle

Dolly T. Seeburger
Email: dseeburger3@gatech.edu

This PDF file includes:

Supporting Information Text

Attention Control Tasks

The four tasks used to measure the individual differences in attention control were the Antisaccade, Selective Visual Arrays, Stroop with an adaptive response deadline, and the Sustained Attention to Cue Task (SACT).

Antisaccade Task (1, 2)

Participants were tasked with identifying either a "Q" or an "O" that appeared briefly on the opposite side of the screen as a visual cue. After a central fixation cross appeared for 1000 ms or 2000 ms, participants heard a brief tone (300 ms) that alerted them to the onset of an asterisk (*), which flashed at a 12.3° visual angle to the left or right of the central fixation for 100 ms. Afterward, the letter “Q” or “O” was presented on the opposite side at 12.3° visual angle of the central fixation for 100 ms, immediately followed by a visual mask (##). Participants had to indicate if they observed the letter as a "Q" or an "O." Participants completed 16 slow practice trials, with letter duration set to 750 ms, followed by 72 test trials. The task was scored based on accuracy as the proportion of correct responses. See **Fig. S1.** for a trial diagram.

Selective Visual Arrays – Orientation Judgement (3, 4)

Following a 1000 ms period of central fixation, a cue word ("RED" or "BLUE") appeared, instructing the participant to focus their attention on either red or blue rectangles. Next, a target array of rectangles, encompassing different orientations (horizontal, left diagonal, right diagonal, and vertical) in both red and blue, was presented for 250 ms. This was followed by a blank screen lasting 900 ms. Next, a probe array with only the cued-color rectangles was presented, with one rectangle highlighted by a white dot. The orientation of the highlighted rectangle was either the same as it was in the target array, or different, with equal likelihood. Participants used the keyboard to indicate whether the orientation of the highlighted rectangle had changed or remained the same. The target array consisted of either 3 or 5 rectangles per color (10 and 14 total). Each array set size had 48 trials. Capacity scores (k) for each array size were computed using the single-probe correction method (5): set size * (hit rate + correction rejection rate – 1). The task performance was scored as the mean k estimate across the two set sizes. See **Fig. S2**. for a trial diagram.

Stroop Task with Adaptive Response Deadline (6, 7)

In this task, the words "RED," "GREEN," and "BLUE" were sequentially presented in red, green, or blue font colors. The words were either congruent with the color (e.g., the word “RED” in red font color) or incongruent with the color (e.g., the word “RED” in blue font color). Participants were instructed to identify the font color by pressing 1, 2, or 3 on the number pad, corresponding to green, blue, and red, respectively. To facilitate response mapping, the keys had colored paper with matching colors taped onto them. There was a 2:1 ratio of congruent to incongruent trials with 96 and 288 trials overall. The task was administered over 4 blocks of 72 trials each with an optional rest break between blocks. Practice trials were administered in each block, with 24 response mapping practice trials, 18 standard Stroop trials without response deadlines, and 18 non-adaptive response deadline practice trials.

An adaptive procedure was employed to determine the participant's response deadline threshold, aiming for approximately 75% accuracy. This deadline adjustment was based solely on trial level accuracy on incongruent trials. On each incongruent trial, if an incorrect response was given or the reaction time exceeded the response deadline, the response deadline was extended (allowing more time to respond) for the subsequent trial. Conversely, if a correct response was made and the reaction time fell below the response deadline, the deadline was reduced (allowing less time to respond) for the next trial. The response deadline started at 1.5 seconds. A 3:1 up-to-down ratio was used for the step sizes such that the step size (change in response deadline) for incorrect/too slow of trials was three times larger than the step size for correct/deadline met trials. The step size started at 240:80 ms, decreased to 120:40 ms after 17 incongruent trials, decreased to 60:20 ms after 33 incongruent trials, decreased to 30:10 ms after 49

incongruent trials, decreased to 15:5 ms after 65 incongruent trials, and finally settled at 9:3 ms after 81 incongruent trials. Feedback was given in the form of an auditory tone and the words “TOO SLOW! GO FASTER!” presented in red font when the response deadline was not met. This feedback remained onscreen for 1,000 ms. This task was scored as the mean threshold value from the last four deadline reversals. See **Fig. S3.** for a trial diagram.

Sustained Attention to Cue Task (6, 8)

In this task, participants needed to sustain their attention at a fixed, cued location for a variable amount of time. Each trial began with a 1,000 ms fixation interval. Following the fixation, a 750 ms interval displayed the words "Get Ready!" at a to-be-cued location, accompanied by an alerting tone. This interval was designed to prepare the participant for the upcoming trial. Subsequently, a large circular cue was presented, which gradually shrank to the point of a to-be-attended location. The circle cue on the screen lasted about 500 milliseconds before it was removed from the display. The display then remained blank over a variable wait interval, which lasted between 0 seconds and 2 to 12 seconds, in 500 ms steps (e.g., 2, 2.5, 3, 3.5… seconds). After the wait interval, an array of letters (B, P, and R) appeared at the cued location, with a target letter displayed in a dark gray at its center. The non-target letters were presented in a silver font and were randomly arranged around the target letter within a 96 × 96-pixel square, with a minimum separation of 24 pixels to prevent overlap. The target array was visible for 250 ms, after which the target letter was masked for 300 ms. After the mask, a response screen with B, P, and R response options appeared, and participants used a mouse to identify the target letter. After a response, there was a blank buffer display presented for 500 ms.

The task consisted of 6 practice trials with feedback. The task had 3 blocks of 22 trials for 66 trials. No feedback was given on the real trials. Each wait interval occurred once per block. There was a self-timed break given after the first and second block of trials. This task was scored as the proportion of correct responses. See **Fig.S4.** for a trial diagram.

Working Memory Capacity Tasks

The three tasks used to measure the individual differences in working memory capacity were the advanced complex span tasks. The “advanced tasks” were used because their larger memory set sizes show better discrimination in high-ability samples (9). The tasks were the Advanced Operation Span, Advanced Symmetry Span, and Advanced Rotation Span tasks.

Advanced Operation Span.

On each trial, participants first solved a mental arithmetic problem (e.g., (3×4) - 6 = 5) by indicating whether the statement was true or false. They were then presented with a single arrow with a to-be-remembered letter. This alternation continued until a variable set-size of letters was presented (set sizes ranged from 3 to 9 letters) participants tried to recall the letters in their correct serial position. There are 14 trials (2 blocks of 7 trials), and each set- size occurs twice (once in each block). The dependent variable is the edit distance score, which, for this task, has a maximum value of 84.

Advanced Symmetry Span

On each trial, participants judged whether a 16×16 grid of black and white squares was symmetrical about the vertical midline. After each symmetry judgement, they were presented with a 4×4 grid with one cell highlighted. The location of the red square was the to-be-remembered spatial location. Participants completed a variable number of alternations (2-7) until a recall screen appeared. Participants then attempted to recall the locations of the red square in their correct serial order. There was a total of 12 trials (2 blocks of 6 trials), set-sizes ranged from 2-7, and each set-size occurred twice (once in each

block). The dependent variable is the edit distance score, which, for this task, has a maximum value of 54.

Advanced Rotation Span
On each trial, participants solved mental rotation problem in which they judged whether a rotated letter faced the correct direction or it was mirror-reversed. Each mental rotation problem was followed by a single arrow with a specific direction (8 possible directions; the four cardinal and four ordinal directions) and specific size (small or large). Both the direction and size of the arrow were the to-be-remembered features. This alternation continued until a variable set-size of arrows was presented, when participants tried to recall the set in their correct serial position. There are 12 trials (2 blocks of 6 trials), set-sizes ranged from 2-7, and each set- size occurs twice (once in each block). Once again, the dependent variable is the edit distance score, which, for this task, has a maximum value of 54 (10). See **Fig. S5.** for a trial diagram.

Note: In each task, subjects respond true/false or yes/no to a processing (distractor) task prior to the presentation of each to-be-remembered stimulus. After a variable amount of presentations (depending on the set-size for that trial), a recall screen appears asking the subject to recall the to-be-remember stimulus in order of presentation.

Fluid Intelligence Tasks
The three tasks used to measure the individual differences in fluid intelligence were the three reasoning tasks of Raven's Advanced Progressive Matrices (RAPM), Number Series, and Letter Sets

Raven's Advanced Progressive Matrices (RAPM)– Odd problems (11)
In this task participants were presented with a matrix of figures that follow a logical pattern across rows and columns. For each problem in this task, a 3 × 3 matrix of 8 abstract figures was presented with the bottom-right element missing. Participants had to identify set of rules relating the 8 figures and select one of eight response options that completed the pattern. Participants were given 10 minutes to solve 18 problems (the odd items from the full test). The dependent variable was the total number of correct solutions in the time allotted.

Number Series (12)
Participants were shown a set of numbers (e.g., 1, 1, 2, 3, 5, 8) on a computer screen. Each number in the sequence was determined by some rule. Participants had to identify the rule and select the next number that should occur next in the sequence from five possible alternatives. In the example above, each number is determined by summing the two that came before it, so the next number in the series should be 13. Participants were given 5 minutes to complete 15 problems. The dependent variable was the total number of correct solutions in the time allotted.

Letter Sets (13)
Participants were shown 5 groups of 4-letter sequences, e.g., NOPQ, DEFL, ABCD, HIJK, and UVWX. The goal was to identify the rule that united four of these groups and indicate which group of letters broke the rul. In the example given above, all letter sets followed consecutive alphabetical order, except for DEFL. Participants were given 10 minutes to solve 30 problems. The dependent variable was the total number of correct solutions in the allotted time.

N-back Tasks
Participants were asked to perform 1 run of 1-back and 1 run of 3-back task while functional scans are acquired. For both tasks, a sequence of letters were presented one at a time on the screen. Subjects

were asked to make a response of “match” if the letter on the current trial was presented n-trials before or “no match” if the letter did not match n-trials before. There were four blocks of each n-back condition, with a 20 second rest block in between each task block. The procedure for the n-back tasks was adapted from Sala-Llonch and colleagues (14)

Behavioral Data Processing

On any given task, missing data were present due to data cleaning and other factors such as a participant not having enough time to complete a task on a given session, and the task program crashing during administration. Data cleaning consisted of 1) removing problematic participants and 2) removing outliers. For the attention control, working memory capacity, and fluid intelligence tasks, problematic participants were detected as having an overall accuracy equal to or less than chance performance and their scores for that task were set to missing. For the complex-span tasks, overall accuracy was assessed based on the processing task (e.g., symmetry judgments for the symmetry span task). Based on this criterion, 3 participants on the Antisaccade and 1 from the SACT were identified as problematic and were removed. For all cognitive tasks, a multi-pass outlier method was used on the task scores. On each pass, z-scores were computed, then univariate outliers were identified as having scores ±3.5 standard deviations or greater from the mean score on that pass, and outlier scores were replaced with missing data. This process for each task was repeated until no further outliers were detected. Based on this procedure, 5 participants on the Operation Span, and 5 on the SACT, and 3 on the StroopDL task were identified and removed.

Figures

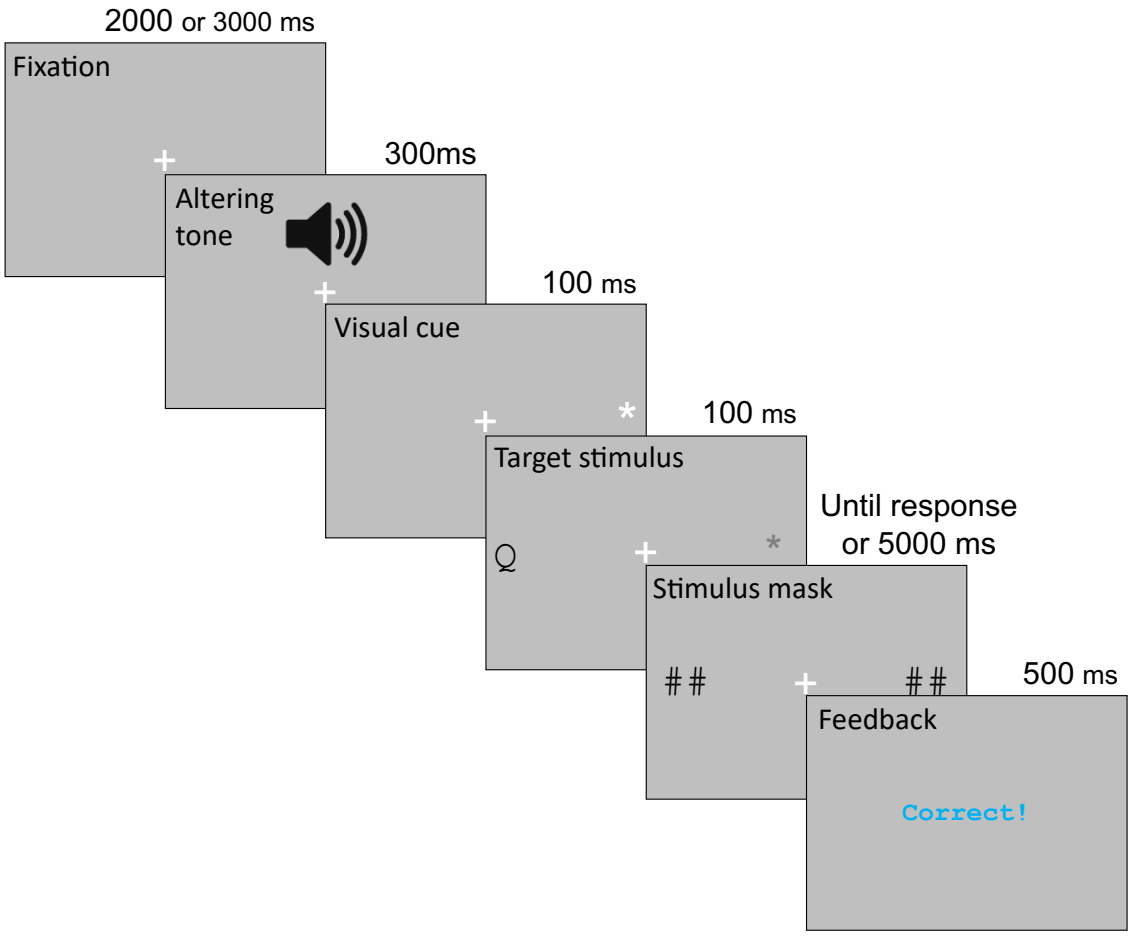

Fig. S1. Diagram of the Antisaccade Task.

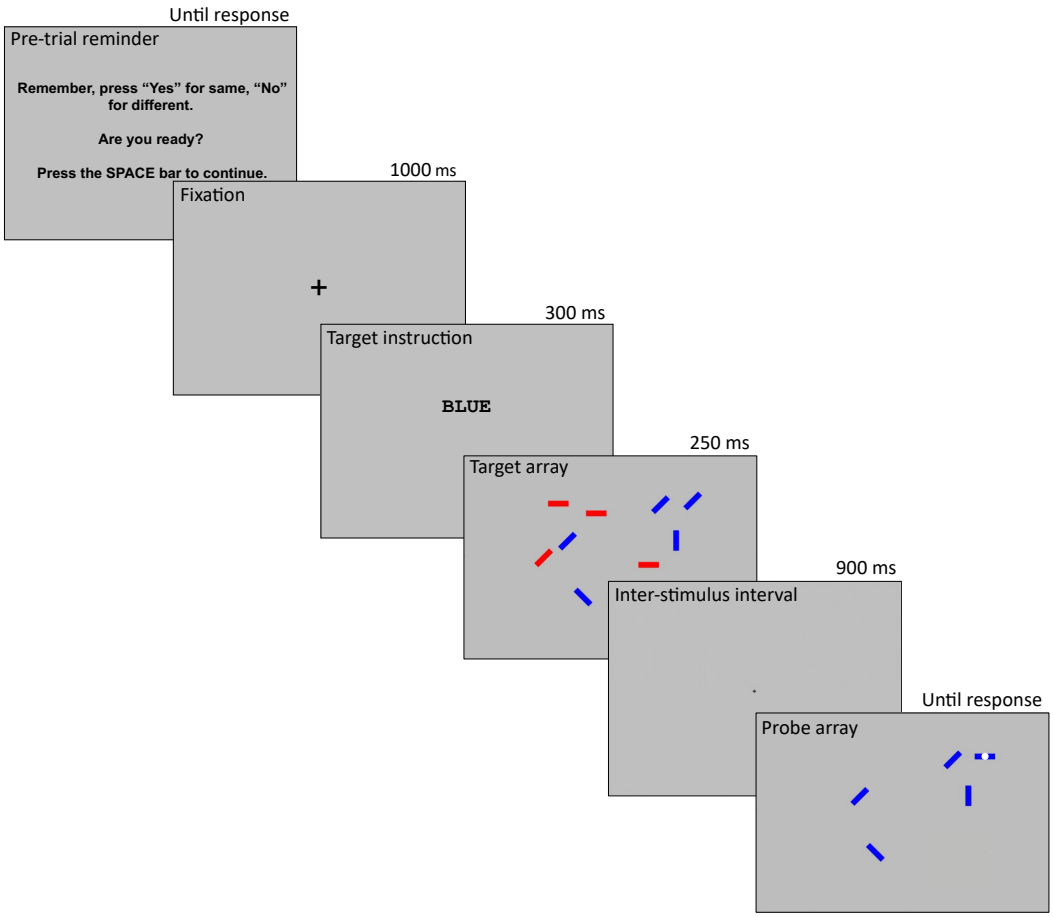

Fig. S2. Diagram of the Selective Visual Arrays—Orientation Judgement Task.

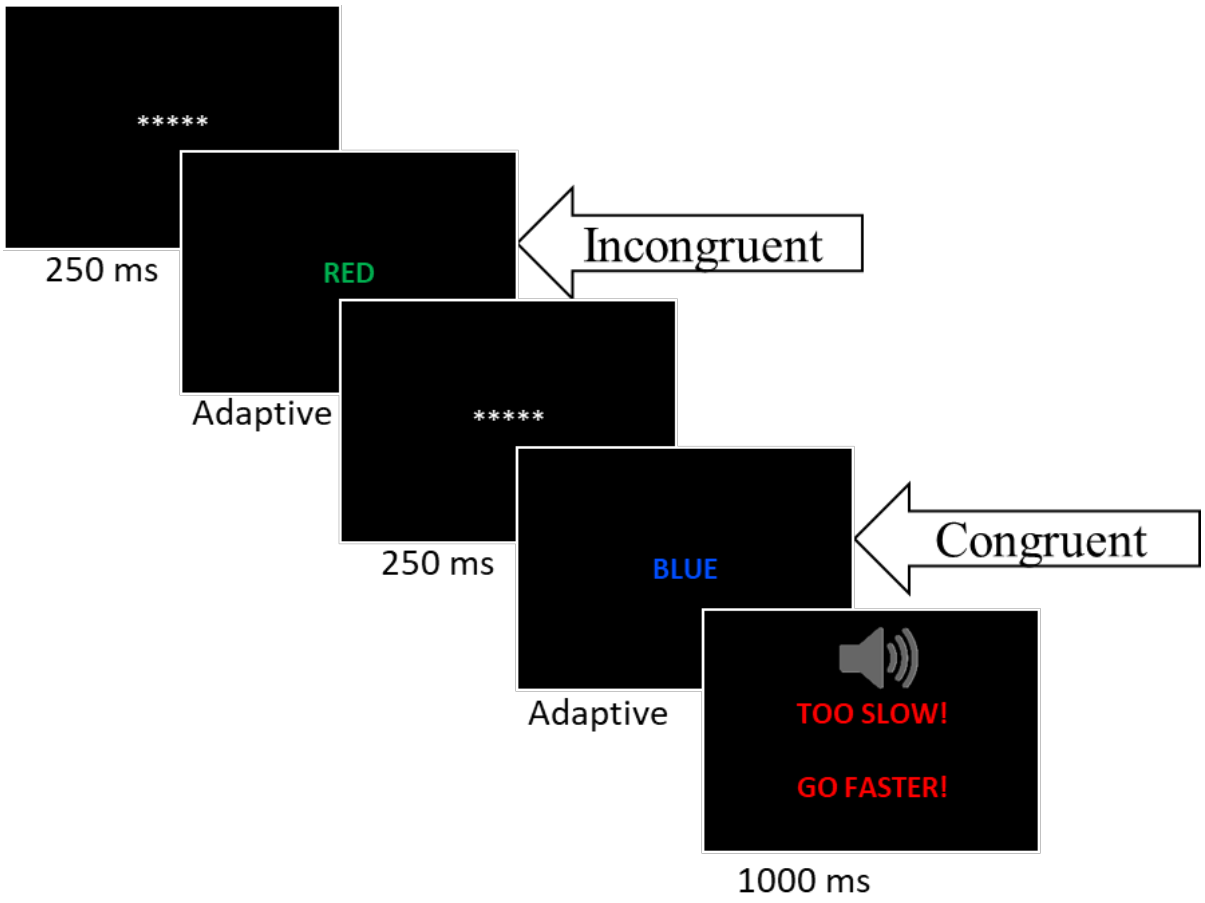

Fig. S3. Diagram of the Adaptive Deadline Color Stroop Task.

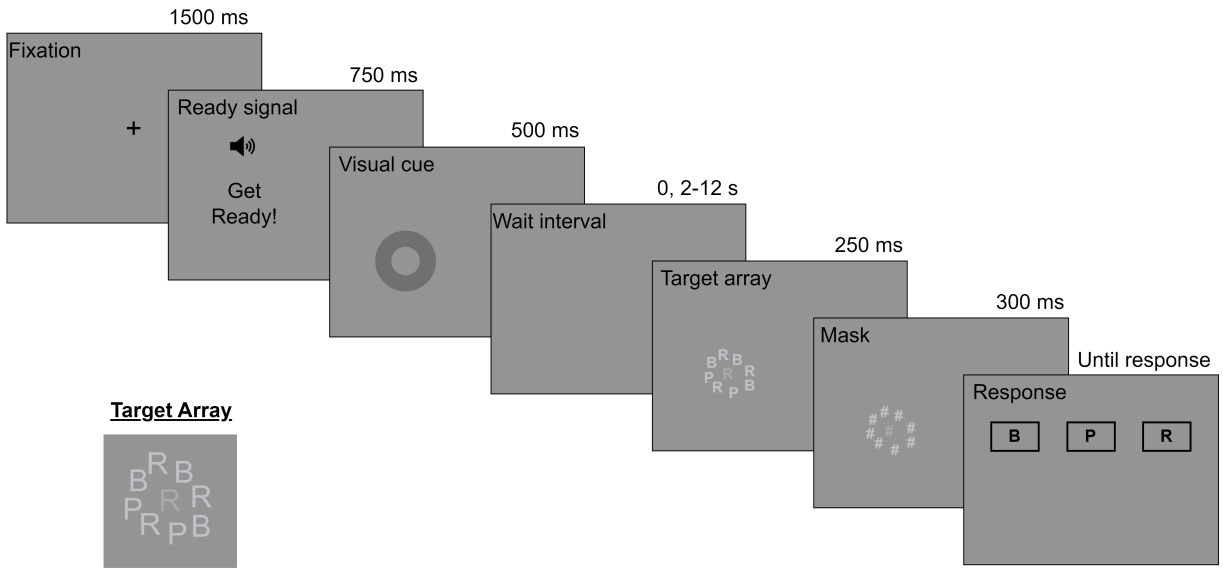

Fig. S4. Diagram of the Sustained Attention to Cue Task.

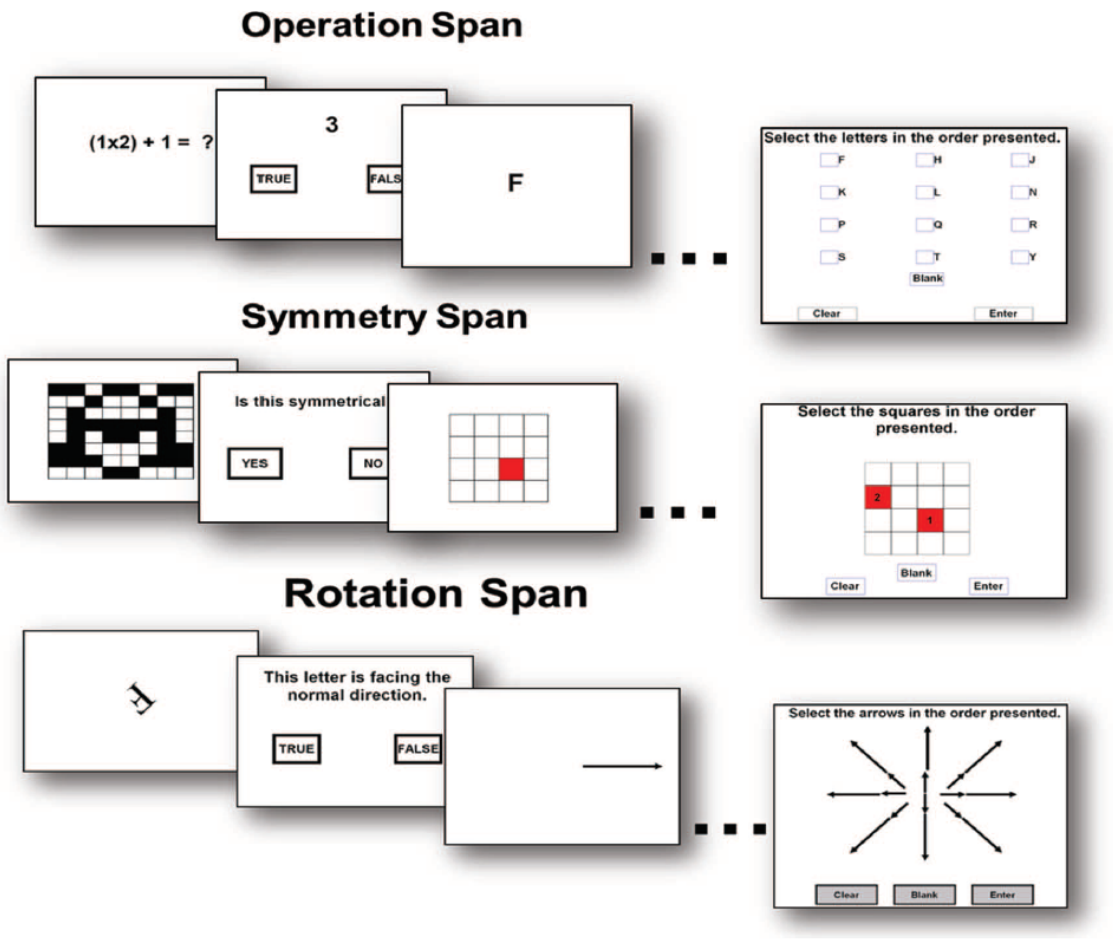

Fig. S5. Diagrams of the Three Complex Span Working Memory Capacity Tasks.

Tables

Table S1. Confirmatory factor analysis. *AC* attention control, *Gf* fluid intelligence, *WMC* working memory capacity, *SACT* Sustained Attention to Cue Task, *StroopDL* Stroop task with an adaptive response deadline, *RAPM* Raven's Advanced Progressive, *SymSpan* Symmetry Span, *RotSpan* Rotation Span

Latent Factor	Task	Loading	95% CI	SE	*z*	*p*
AC	Antisaccade	0.695	0.629 – 0.760	0.033	20.886	0.000
AC	SACT	0.490	0.356 – 0.625	0.069	7.141	<0.001
AC	StroopDL	−0.413	−0.549 – −0.277	0.069	−5.962	<0.001
AC	VisualArrays	0.813	0.741 – 0.886	0.037	21.956	0.000
Gf	LetterSets	0.556	0.431 – 0.681	0.064	8.742	0.000
Gf	NumberSeries	0.623	0.510 – 0.736	0.058	10.831	0.000
Gf	RAPM	0.771	0.680 – 0.862	0.047	16.555	0.000
WMC	OSpan	0.539	0.418 – 0.660	0.062	8.710	0.000
WMC	RotSpan	0.782	0.703 – 0.861	0.040	19.413	0.000
WMC	SymSpan	0.807	0.730 – 0.883	0.039	20.600	0.000

Table S2. Correlations between the estimated factors. *AC* attention control, *Gf* fluid intelligence, *WMC* working memory capacity. Unique scores are latent factor scores residualized by removing shared variance with the other latent factors. Z indicate unique z-scores.

	AC	WMC	Gf	AC unique z	WMC unique z	Gf unique z
AC	1.000					
WMC	0.619***	1.000				
Gf	0.596***	0.565***	1.000			
AC unique z	0.727***	0.001	0.001	1.000		
WMC unique z	-0.000	0.746***	-0.001	-0.425***	1.000	
Gf unique z	-0.001	-0.002	0.762***	-0.379***	-0.313***	1.000

Computed correlation used pearson-method with listwise-deletion.
* $p < .05$; ** $p < .01$; *** $p < .001$

SI References

1. P. E. Hallett, Primary and secondary saccades to goals defined by instructions. *Vision Res.* **18**, 1279–1296 (1978).
2. K. A. Hutchison, Attentional control and the relatedness proportion effect in semantic priming. *J. Exp. Psychol. Learn. Mem. Cogn.* **33**, 645–662 (2007).
3. N. Cowan, E. M. Elliott, J. S. Saults, C. C. Morey, S. Mattox, A. Hismjatullina, A. R. A. Conway, On the capacity of attention: Its estimation and its role in working memory and cognitive aptitudes. *Cogn. Psychol.* **51**, 42–100 (2005).
4. C. Draheim, J. S. Tsukahara, R. W. Engle, Replication and extension of the toolbox approach to measuring attention control. *Behav. Res. Methods* **56**, 2135–2157 (2023).
5. J. R. Stroop, Studies of interference in serial verbal reactions. *J. Exp. Psychol.* **18**, 643–662 (1935).
6. J. S. Tsukahara, R. W. Engle, Sustaining the focus of attention and how it relates to performance in complex cognitive tasks. PsyArXiv, https://doi.org/10.31234/osf.io/wd5kz (2023).
7. C. Draheim, T. L. Harrison, S. E. Embretson, R. W. Engle, What item response theory can tell us about the complex span tasks. *Psychol. Assess.* **30**, 116–129 (2018).
8. C. Gonthier, An easy way to improve scoring of memory span tasks: The edit distance, beyond "correct recall in the correct serial position." *Behav. Res. Methods* **16**, (2022).
9. J. C. Raven, J. H. Court, *Raven's Progressive Matrices and Vocabulary Scales* (Oxford Psychologists Press, Oxford, UK, 1998).
10. L. L. Thurstone, *Primary Mental Abilities* (University of Chicago Press, Chicago, 1938).
11. R. B. Ekstrom, J. W. French, H. H. Harman, D. Dermen, *Manual for Kit of Factor Referenced Cognitive Tests* (Educational Testing Service, Princeton, NJ, 1976).
12. R. Sala-Llonch, C. Peña-Gomez, E. M. Arenaza-Urquijo, D. Vidal-Piñeiro, N. Bargalló, C. Junqué, D. Bartrés-Faz, Brain connectivity during resting state and subsequent working memory task predicts behavioural performance. *Cortex* **48**, 1187–1196 (2012).